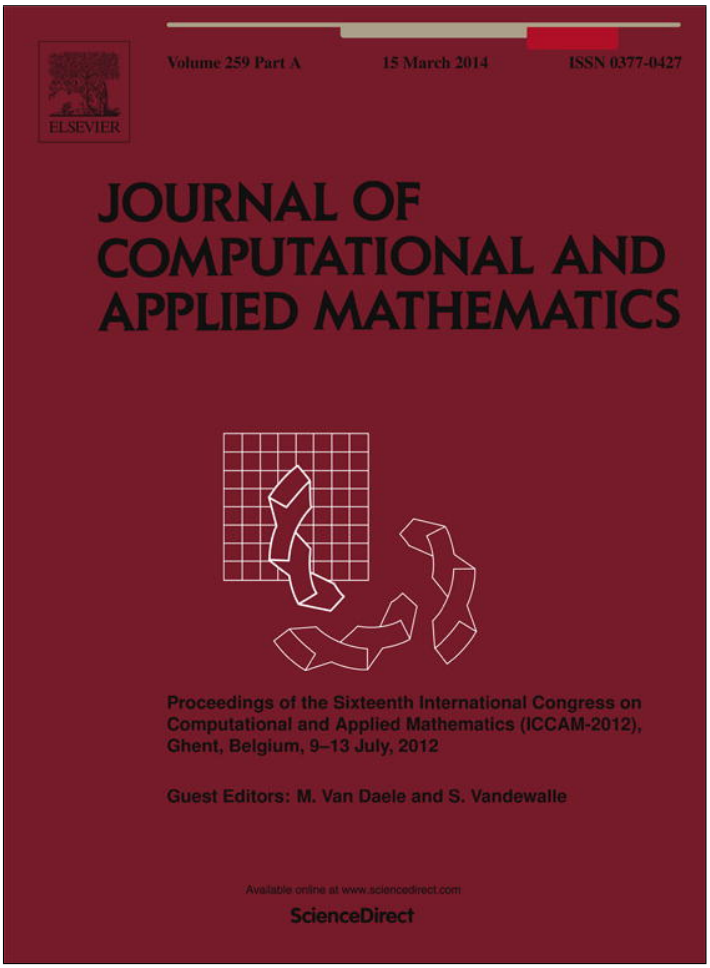

Journal of Computational and Applied Mathematics 259 (2014) 57–64

Contents lists available at ScienceDirect

Journal of Computational and Applied Mathematics

journal homepage: www.elsevier.com/locate/cam

Derivative-optimized empirical mode decomposition for the Hilbert–Huang transform

Peter C. Chu [a,*], Chenwu Fan [a], Norden Huang [b]

[a] Naval Ocean Analysis and Prediction Laboratory, Department of Oceanography, Naval Postgraduate School, Monterey, CA, USA

[b] Research Center for Adaptive Data Analysis, National Central University, Chungli, Taiwan

ARTICLE INFO

Article history:
Received 20 August 2012
Received in revised form 23 February 2013

Keywords:
Derivative-optimized empirical mode decomposition (DEMD)
Hilbert–Huang transform (HHT)
Hermitian polynomials
Intrinsic mode function (IMF)
End effect
Detrend uncertainty

ABSTRACT

In the empirical mode decomposition (EMD) for the Hilbert–Huang transform (HHT), a nonlinear and non-stationary signal is adaptively decomposed by an HHT into a series of intrinsic mode functions (IMFs) with the lowest one as the trend. At each step of the EMD, the low-frequency component is mainly determined by the average of the upper envelope (consisting of local maxima) and the lower envelope (consisting of local minima). The high-frequency component is the deviation of the signal relative to the low-frequency component. The fact that no local maximum and minimum can be determined at the two end-points leads to detrend uncertainty, and in turn causes uncertainty in the HHT. To reduce such uncertainty, Hermitian polynomials are used to obtain the upper and lower envelopes with the first *derivatives* at the two end-points (q_L, q_R) as parameters, which are optimally determined on the base of minimum temporal variability of the low-frequency component in the each step of the decomposition. This well-posed mathematical system is called the Derivative-optimized EMD (DEMD). With the DEMD, the end effect, and detrend uncertainty are drastically reduced, and scales are separated naturally without any *a priori* subjective selection criterion.

Published by Elsevier B.V.

1. Introduction

Analysis of non-stationary time series in terms of nonlinear dynamics has drawn attention in many disciplines. Traditional methods, based on linear and stationary assumptions, are not suitable for analyzing nonlinear and non-stationary data. The Hilbert–Huang transform (HHT) with adaptive empirical mode decomposition (EMD) [1] has been developed to analyze nonlinear/non-stationary data. Being adaptive means that the definition of basis functions has to be data dependent, not *a priori* defined (e.g., sinusoidal functions in linear/stationary time series analysis).

EMD decomposes a nonlinear and non-stationary signal into several intrinsic mode functions (IMFs) with the lowest varying IMF as the trend. Instantaneous frequency and then the time–frequency–energy distribution characteristics can be obtained by the HHT. An IMF is a function that must satisfy two conditions according to the EMD algorithm originally developed: (a) the difference between the number of local extrema and the number of zero-crossings must be zero or one; (b) the running mean value of the envelope defined by the local maxima and the envelope defined by the local minima is zero. The average of the upper and lower envelopes is treated as the low-frequency component. The deviation of original signal versus the low-frequency component is regarded as the high-frequency component. Thus, accurate determination of two envelopes (i.e., one for local maxima and the other for local minima) is crucial for the success of EMD in nonlinear/non-stationary data analysis. For a time series, the interior extrema are easily identified. However, these extrema are not enough

* Corresponding author.
E-mail addresses: pcchu@nps.edu, p_c_chu@yahoo.com (P.C. Chu).

0377-0427/$ – see front matter. Published by Elsevier B.V.
http://dx.doi.org/10.1016/j.cam.2013.03.046

to determine two well-behaved fitting spline envelopes near the two end-points since no local maximum/minimum can be identified there.

The easiest way is to treat the two end-points as "frozen" points, i.e. the two end-points are on both the maximum envelope and the minimum envelope. Such a treatment makes the trend varying from the first end-point to the last end-point. Another practice is to extend the data points beyond the end-points so as to carry out the spline envelope fitting over and even beyond the existing data range; examples are the wave extension method [1], the local straight-line extension method [2], mirror or anti-mirror extension [3], self-similarity [4], overlapping sliding windows [5], and rejecting segments close to the end-points [2]. While methods for extending data vary, the essence of these methods is to predict data beyond the end-points, a dauntingly difficult procedure even for linear and stationary processes. Since the original signal only has the extrema in the data series, extending points beyond the two end-points is not *realistic*. Therefore the data extension methods will not solve the problem no matter how much effort has been spent. Besides, the end error may propagate from the ends to the interior of the data span, which would cause severe deterioration of the IMFs obtained.

A more recent approach to deal with uncertainties in EMD is to use some postprocessing that allows the sum of all IMFs to be *different* from the original signal. For instance, the signal is approximately represented by a linear combination of original IMFs with weighting parameters, which are determined using the least square error relative to the original signal. This algorithm is called optimal EMD (OEMD) for one-dimensional weights and bidirectional optimal EMD (BOEMD) for two-dimensional weight matrix so as to facilitate approximation by window-based filtering [6]. However, OEMD and BOEMD are limited by their block-based nature, and use of adaptive filters was proposed [7]. The major weakness of this type of approach is the inequality between the sum of all IMFs and the original signal.

Questions arise: Can the upper and lower envelopes be determined in a systematic way? Can the local maximum and minimum be objectively and optimally determined at the two end-points without using either extrapolation or interpolation (with an extra point beyond the end-point)? Can the sum of all IMFs always equal the original signal? These problems will be solved in this study through using compact difference concepts [8–10] with Hermitian polynomials. The upper and lower envelopes are obtained with the *first derivatives* at the two end-points (q_L, q_R) as parameters, which are optimally determined on the base of minimum temporal variability of the low-frequency component in each step of the decomposition. This method, called derivative-optimized EMD (DEMD), shows evident improvement in the EMD analysis.

The rest of the paper is organized as follows. Section 2 introduces the classical EMD for the Hilbert–Huang transform (HHT). Section 3 describes the construction of upper and lower envelopes using Hermitian polynomials with the first derivatives at the two end-points, q_L (at t_1) and q_R (at t_N), as tuning parameters. Section 4 depicts optimal determination of (q_L, q_R) on the base of minimum temporal variability for the low-frequency component. Section 5 shows the evaluation. Section 6 presents the conclusions.

2. HHT

The HHT has two steps. First, the process of empirical mode decomposition (EMD) reduces the time series under analysis into components, known as intrinsic mode functions (IMFs). Let a real signal $x(t)$ be defined in the time interval $[t_1, t_N]$ with two end-points $x_1 = x(t_1)$ and $x_N = x(t_N)$. The EMD method is depicted as follows. First, the local minima $(x_j^{(\min)}, j = 1, 2, \ldots, J)$ and local maxima $(x_k^{(\max)}, k = 1, 2, \ldots, K)$ of the signal $x(t_i)$ are identified with $J = K$ or differing at most by 1. Second, interpolation/extrapolation methods are used to determine the upper and lower envelopes $[u(t), l(t)]$ for $t \in [t_1, t_N]$. The mean of the two envelopes is calculated:

$$m(t) = [u(t) + l(t)]/2. \tag{1}$$

The mean is subtracted from the signal, providing the high-frequency component (Fig. 1),

$$h(t) = x(t) - m(t), \tag{2}$$

which is then checked to see if it satisfies the above two conditions to be an IMF. If yes, it is considered as the first IMF, and denoted

$$c(t) = h(t). \tag{3}$$

It is subtracted from the original signal, and the first residual,

$$r(t) = x(t) - c(t), \tag{4}$$

is taken as the new series to continue the decomposition. If $h(t)$ is not an IMF, a procedure called a "sifting process" is applied as many times as necessary to obtain an IMF. In the sifting process, $h(t)$ is considered as the new data, and the same procedure applies. The IMFs are orthogonal (or almost orthogonal) functions (mutually uncorrelated). This method does not require stationarity and linearity of the data and is especially suitable for non-stationary and nonlinear time series analysis. By construction, the number of extrema decreases when going from one residual to the next; the above algorithm ends when the residual has only one extremum, or is constant, and in this case no more IMFs can be extracted; the complete decomposition is then achieved in a finite number of steps. The signal $x(t)$ is finally written as

$$x(t) = \sum_{p=1}^{P} c_p(t) + r_P(t), \tag{5}$$

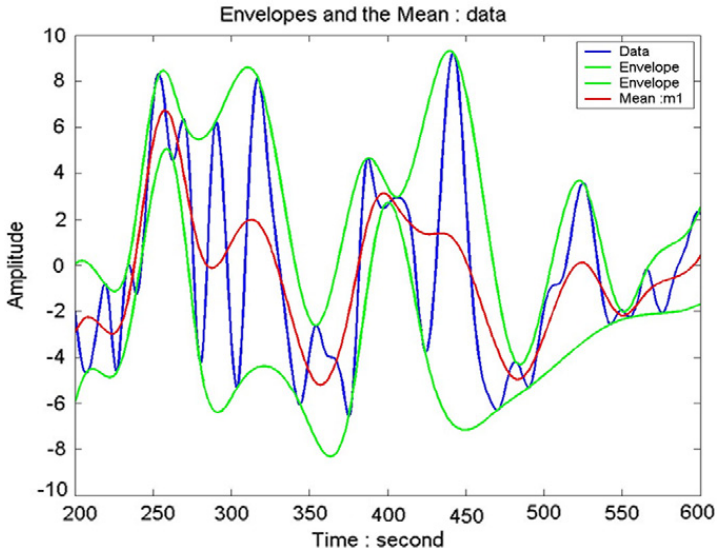

Fig. 1. Procedure of traditional EMD.

where $c_p(t)$ is the pth IMF and $r_P(t)$ is the residual, with no any oscillation (i.e., non-existence of both maximum and minimum envelopes), which is the trend.

The Hilbert transform is conducted on each IMF $c_p(t)$,

$$z_p(t) = c_p(t) + \mathrm{i}\hat{c}_p(t), \tag{6}$$

where $\mathrm{i} \equiv \sqrt{-1}$ and $\hat{c}_p(t)$ is the Hilbert transform of $c_p(t)$, represented by

$$\hat{c}_p(t) = \frac{1}{\pi} CP \int_{-\infty}^{+\infty} \frac{c_p(s)}{t-s} ds, \tag{7}$$

where CP is the Cauchy principal value of the integral. The complex variable $z_p(t)$ in (6) can be rewritten as

$$z_p(t) = c_p(t) + \mathrm{i}\hat{c}_p(t) = a_p(t) \exp[\mathrm{i}\theta_p(t)], \tag{8}$$

to obtain the instantaneous amplitude $a_p(t)$ and the instantaneous phase function $\theta_p(t)$, and the instantaneous frequency is calculated by

$$\omega_p(t) = d\theta_p(t)/dt. \tag{9}$$

Recently, it has been discovered that the Hilbert transform has a severe limitation on the data for instantaneous frequency computation. Different methods such as direct quadrature and the normalized Hilbert transform have been discussed in detail; see [10,11].

The Hilbert transform conducted on each IMF, $c_p(t)$, is called the Hilbert–Huang transform (HHT) [1]. The key issue in the EMD method for the HHT is the accurate determination of the upper and lower envelopes $\{u_p(t), l_p(t)\}$. It is noted that the values of $\{u_p(t), l_p(t)\}$ are only given at the local maxima $(x_k^{(\max)}, k = 1, 2, \ldots, K)$, and local minima $(x_j^{(\min)}, j = 1, 2, \ldots, J)$, and are unknown at the other time instances, especially at the two end-points t_1 and t_N (Fig. 1). This causes uncertain in determining $c_p(t)$ with two long-recognized difficulties: end-point effect, and detrend uncertainty.

3. Hermitian polynomials for upper and lower envelopes

Let the signal be discretized as $\{x(t_i), i = 1, 2, \ldots, N\}$, and let $(\tau_1, \tau_2, \ldots, \tau_M)$ represent occurrence time instances for either local maxima $(t_1^{\max}, t_2^{\max}, \ldots, t_K^{\max})$, or local minima $(t_1^{\min}, t_2^{\min}, \ldots, t_J^{\min})$, as shown in Fig. 2. Let e_m represent the local maximum (or minimum) with q_m its first derivative at time instance τ_m $(m = 1, 2, \ldots, M)$, and let $\Delta_m = \tau_{m+1} - \tau_m$, $\xi = (t - \tau_m)/\Delta_m$. A cubic spline

$$p_3(\xi) = \phi_1(\xi)\, e_m + \phi_2(\xi)\, e_{m+1} + \phi_3(\xi)\, q_m \Delta_m + \phi_4(\xi)\, q_{m+1} \Delta_m, \tag{10}$$

is used to fill the gap between two neighboring local maxima (minima) between t_m^a and t_{m+1}^a with given values of e_m and q_m. This spline has the following features:

$$p_3(0) = e_m, \qquad p_3(1) = e_{m+1}, \qquad dp_3(0)/dt = q_m, \qquad dp_3(1)/dt = q_{m+1}. \tag{11}$$

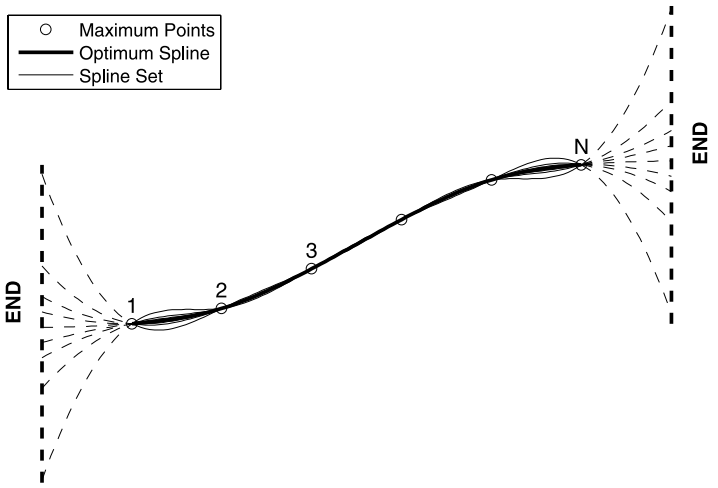

Fig. 2. Uncertain upper (or lower) envelope at the two end-points.

Here, $\phi_1(\xi)$, $\phi_2(\xi)$, $\phi_3(\xi)$, $\phi_4(\xi)$ are defined by [5]

$$\phi_1(\xi) = 1 - 3\xi^2 + 2\xi^3, \qquad \phi_2(\xi) = 3\xi^2 - 2\xi^3,$$
$$\phi_3(\xi) = \xi - 2\xi^2 + \xi^3, \qquad \phi_4(\xi) = \xi^3 - \xi^2. \tag{12}$$

Let the second derivative of $e(t)$ be continuous at each local maximum (or minimum) time instance, τ_m ($m = 2, 3, \ldots, M-1$),

$$d^2e/dt^2|_{(\tau_m-0)} = d^2e/dt^2|_{(\tau_m+0)}. \tag{13}$$

Substitution of (10) into (13) leads to the compact difference schemes [8,9],

$$\Delta_m q_{m-1} + 2\left(\Delta_{m-1} + \Delta_m\right) q_m + \Delta_{m-1} q_{m+1} = 3\left(\Delta_m \frac{\Delta e_{m-1}}{\Delta_{m-1}} + \Delta_{m-1}\frac{\Delta e_m}{\Delta_m}\right), \quad \Delta e_m = e_{m+1} - e_m \tag{14}$$

where $m = 2, 3, \ldots, M-1$. Since the value of $e(t)$ is unknown at the two end-points (Fig. 2), the condition (14) cannot be satisfied at the first and last local maximum (minimum) time instances τ_1 and τ_M.

The values and derivatives of the local maximum (or minimum) at the two end-points, $[e(t_1), e(t_N), e'(t_1), e'(t_N)]$, are unknown. To overcome this, only the first derivative at t_1 (q_L) along with both the value and the first derivative at $\tau_1(e_1, q_1)$ are used to fill the gap between t_1 and τ_1 with a quadratic spline,

$$p_2(\zeta) = \psi_1(\zeta)e_1 + \psi_2(\zeta)q_L\Delta_L + \psi_3(\zeta)q_1\Delta_L, \quad \zeta = (t - t_1)/\Delta_L,\ \Delta_L = \tau_1 - t_1, \tag{15}$$

where

$$\psi_1(\zeta) = 1, \qquad \psi_2(\zeta) = \left(-1 + 2\zeta - \zeta^2\right)/2, \qquad \psi_3(\zeta) = \left(\zeta^2 - 1\right)/2. \tag{16}$$

This spline has the following features:

$$p_2(1) = e_1, \qquad dp_2(0)/dt = q_L, \qquad dp_2(1)/dt = q_1. \tag{17}$$

Continuity of the second derivative (13) at the first local maximum (or minimum) time instance (t_1) from ($t_1 - 0$) [using the quadratic spline (15)] to ($t_1 + 0$) [using the cubic spline (10)] leads to

$$-\Delta_1 q_L + \left(4\Delta_L + \Delta_1\right) q_1 + 2\Delta_L q_2 = 6\Delta_L \frac{e_2 - e_1}{\Delta_1}. \tag{18}$$

A similar algebraic equation is obtained for the end-point t_N:

$$2\Delta_R q_{M-1} + \left(4\Delta_R + \Delta_{M-1}\right) q_M - \Delta_{M-1} q_R = 6\Delta_R \frac{e_M - e_{M-1}}{\Delta_{M-1}}, \quad \Delta_R = t_N - \tau_M, \tag{19}$$

where q_R is the first derivative at the right end-point. Fig. 2 shows the variation of the spline with different values of q_L and q_R. For simplicity, without loss of generality, the upper and lower envelopes are assumed to have the same first derivatives (q_L, q_R) at the two end-points (see Fig. 3).

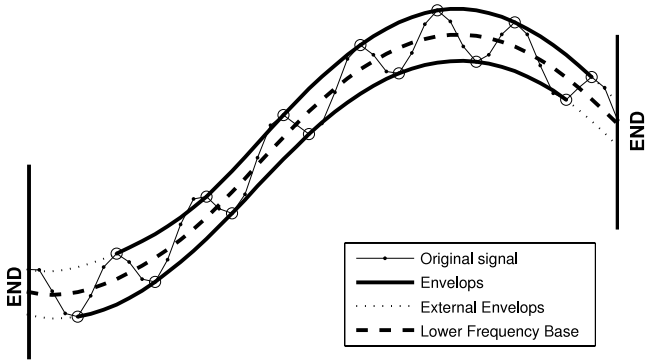

Fig. 3. Optimal determination of (q_L, q_R) by minimal temporal variability for the upper (or lower) envelope, i.e., minimal integrated square of the third derivative (solid curves).

4. Optimal determination of (q_L, q_R)

Eqs. (14), (18) and (19) represent two sets of tri-diagonal linear equations for the first derivatives at the local maximum points of the upper envelope $(q_k^u,\ k = 1, 2, 3, \ldots, K)$ and the lower envelope $(q_j^l,\ j = 1, 2, 3, \ldots, J)$ as the dependent variables. Let the solutions for the upper envelope be given by

$$q_k^u = a_k^u + b_k^u q_L + c_k^u q_R, \quad k = 1, 2, 3, \ldots, K \tag{20}$$

and those for the lower envelope be given by

$$q_j^l = a_j^l + b_j^l q_L + c_j^i q_R, \quad i = 1, 2, 3, \ldots, J. \tag{21}$$

At each step, EMD decomposes the signal into high-frequency and low-frequency components, with the average of the upper and lower envelopes using Eq. (1), i.e., $m(t)$, as the low-frequency component and the deviation from the low-frequency component as the high-frequency component. Thus, the low-frequency component, $m(t)$, should have minimum temporal variability. Usually, small absolute values of derivatives mean small temporal variation. Since the first and second derivatives are already used in obtaining the upper and lower envelopes [see Eqs. (13), (14)], minimization of integrated squared values of the third derivatives,

$$S = \int_{t_1}^{t_N} \left[\frac{d^3u}{dt^3}\right]^2 dt + \int_{t_1}^{t_N} \left[\frac{d^3l}{dt^3}\right]^2 dt \to \min, \tag{22}$$

is used to determine (q_L, q_R). Here, the third derivatives are calculated numerically by

$$\begin{aligned}
\left(\frac{d^3u}{dt^3}\right)_k &= 6\left(2\frac{u_k - u_{k+1}}{\left(\Delta_k^u\right)^3} + \frac{1}{\left(\Delta_k^u\right)^2}\left(a_k^u + a_{k+1}^u + \left(b_k^u + b_{k+1}^u\right) q_L + \left(c_k^u + c_{k+1}^u\right) q_R\right)\right) = F_k(q_L, q_R) \\
\left(\frac{d^3l}{dt^3}\right)_j &= 6\left(2\frac{l_j - l_{j+1}}{\left(\Delta_j^l\right)^3} + \frac{1}{\left(\Delta_j^l\right)^2}\left(a_j^l + a_{j+1}^l + \left(b_j^l + b_{j+1}^l\right) q_L + \left(c_j^l + c_{j+1}^l\right) q_R\right)\right) = G_j(q_L, q_R),
\end{aligned} \tag{23}$$

which are constant in the time interval $[t_k, t_k + 1]$ for the upper envelope and the time interval $[t_j, t_j + 1]$ for the lower envelope since the cubic spline (10) and quadratic spline (15) are used. Substitution of (23) into (22) leads to

$$S = \sum_{k=1}^{K} \left[F_k(q_L, q_R)\right]^2 \Delta_k + \sum_{j=1}^{J} \left[G_j(q_L, q_R)\right]^2 \Delta_j. \tag{24}$$

The end-point derivatives (q_L, q_R) are determined by the minimization of S,

$$\frac{\partial S}{\partial q_L} = 0, \qquad \frac{\partial S}{\partial q_R} = 0, \tag{25}$$

which leads to the following set of linear algebraic equations:

$$\begin{bmatrix} A_{11} & A_{12} \\ A_{21} & A_{22} \end{bmatrix} \begin{bmatrix} q_L \\ q_R \end{bmatrix} = \begin{bmatrix} B_1 \\ B_2 \end{bmatrix}. \tag{26}$$

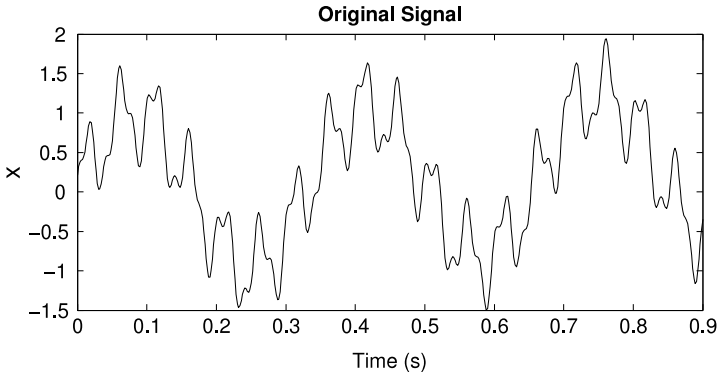

Fig. 4. Time series $\{x_i\}$ represented by Eq. (27).

Table 1
Values of parameters used in Eq. (27).

k	0	3	2	1
A_k	0.5	1.0	0.5	0.20
ω_k		6π (3 Hz)	40π (20 Hz)	100π (50 Hz)
φ_k		0.01	0	0.005

Here,

$$A_{11} = \sum_{k=1}^{K-1} \frac{1}{\left(\Delta_k^u\right)^3} \left(b_k^u + b_{k+1}^u\right)^2 + \sum_{j=1}^{J-1} \frac{1}{\left(\Delta_j^l\right)^3} \left(b_j^l + b_{j+1}^l\right)^2$$

$$A_{12} = A_{21} = \sum_{k=1}^{K-1} \frac{1}{\left(\Delta_k^u\right)^3} \left(c_k^u + c_{k+1}^u\right)\left(b_k^u + b_{k+1}^u\right) + \sum_{j=1}^{J-1} \frac{1}{\left(\Delta_j^l\right)^3} \left(c_j^l + c_{j+1}^l\right)\left(b_j^l + b_{j+1}^l\right)$$

$$A_{22} = \sum_{k=1}^{K-1} \frac{1}{\left(\Delta_k^u\right)^3} \left(c_k^u + c_{k+1}^u\right)^2 + \sum_{j=1}^{J-1} \frac{1}{\left(\Delta_j^l\right)^3} \left(c_j^l + c_{j+1}^l\right)^2$$

$$B_1 = \sum_{k=1}^{K-1} \frac{1}{\left(\Delta_k^u\right)^3} \left(b_k^u + b_{k+1}^u\right)\left(2\frac{u_{k+1}^u - u_k^u}{\Delta_k^u} - \left(a_k^u + a_{k+1}^u\right)\right) + \sum_{j=1}^{J-1} \frac{1}{\left(\Delta_j^l\right)^3} \left(b_j^l + b_{j+1}^l\right)\left(2\frac{u_{j+1}^l - u_j^l}{\Delta_j^l} - \left(a_j^l + a_{j+1}^l\right)\right)$$

$$B_2 = \sum_{k=1}^{K-1} \frac{1}{\left(\Delta_k^u\right)^3} \left(c_k^u + c_{k+1}^u\right)\left(2\frac{u_{k+1}^u - u_k^u}{\Delta_k^u} - \left(a_k^u + a_{k+1}^u\right)\right) + \sum_{j=1}^{J-1} \frac{1}{\left(\Delta_j^l\right)^3} \left(c_j^l + c_{j+1}^l\right)\left(2\frac{u_{j+1}^l - u_j^l}{\Delta_j^l} - \left(a_j^l + a_{j+1}^l\right)\right).$$

As soon as the end-point derivatives (q_L, q_R) are calculated, the upper and lower envelopes are determined. The EMD can be effectively conducted.

5. Example

A time series of $\{x_i\}$ (Fig. 4) consisting of a quadratic trend and three harmonics,

$$x(t_i) = f_0(t_i) + \sum_{k=1}^{3} f_k(t_i), \qquad f_0(t_i) = A_0 t_i^2, \qquad f_k(t_i) = A_k \sin(\omega_k t_i + \varphi_k), \quad k = 1, 2, 3$$

$$x_i = x(t_i), \qquad t_i = (i-1)\Delta t, \qquad t_1 = 0, \qquad t_N = 0.9\ \text{s}, \qquad \Delta t = 0.0018\ \text{s}, \quad N = 501, \tag{27}$$

is used to demonstrate the capability of DEMD. The parameters in (27) are given in Table 1. The left panels of Fig. 5 show the trend and three harmonics of the data represented by (27): $f_{0i} = f_0(t_i), f_{1i} = f_1(t_i), f_{2i} = f_2(t_i)$, and $f_{3i} = f_3(t_i)$. Obviously, only $f_0(t_i)$ represents the trend of the signal $\{x_i\}$. The trend of $\{x_i\}$ varies from f_{01} to f_{0N}:

$$f_{01} = 0, \qquad f_{0N} = 0.405. \tag{28}$$

The DEMD is conducted on the time series $\{x_i\}$ (Fig. 4) to obtain three IMFs and a trend (right panels of Fig. 5). Obviously, the IMFs correspond well to the harmonics, $c_i(t)$ versus $f_i(t)$, with high correlation coefficients (CCs) (0.978 between c_1 and f_1, 0.992 between c_2 and f_2, 0.999 between c_3 and f_3, and 1.0 between the two trends) and low relative root mean square errors (RRMSEs) (0.00394 between c_1 and f_1, 0.0218 between c_2 and f_2, 0.00542 between c_3 and f_3, and 0.0184 between the two trends).

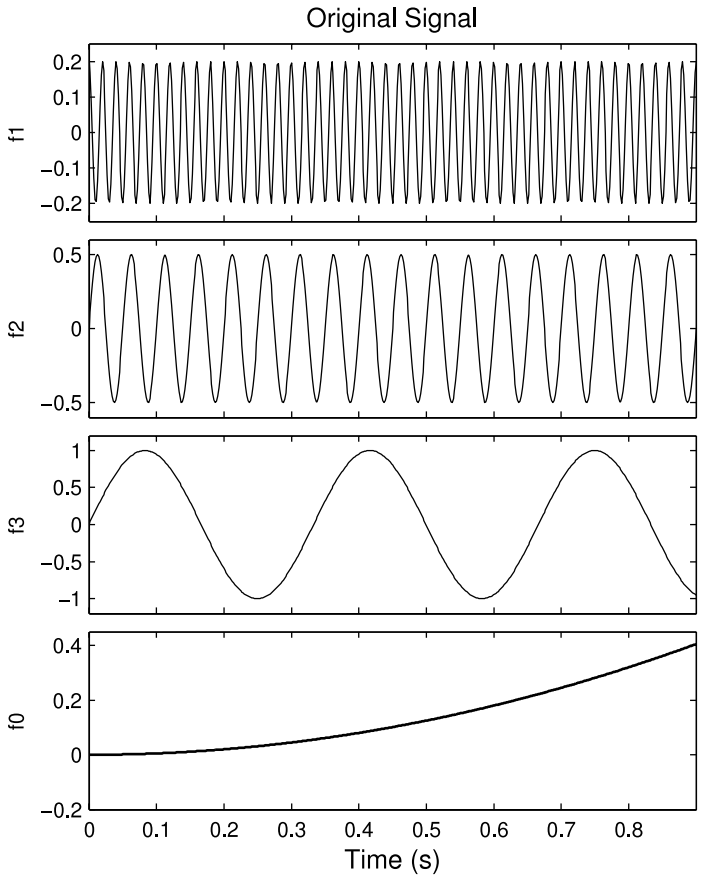

Fig. 5. Components of time series $\{x_i\}$: a quadratic trend and four harmonics given by Eq. (27).

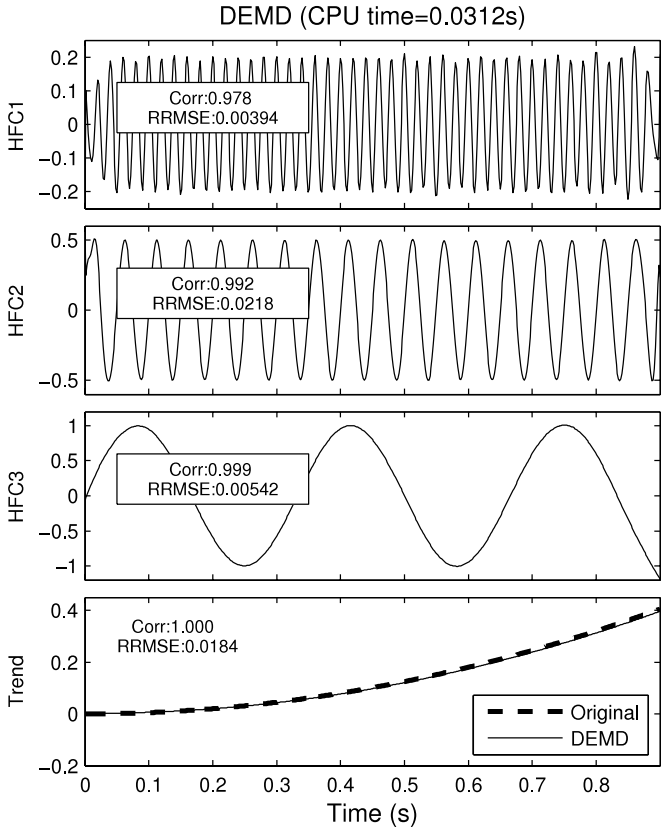

Fig. 6. DEMD on the signal shown in Fig. 5: (a) IMF-1, (b) IMF-2, (c) IMF-3, and (d) trend. Comparison between Figs. 6 and 5 shows the capability to reduce the end effect and detrend uncertainty.

6. Conclusions

(1) A major difficulty in using the HHT (i.e., unknown local maximum and minimum at the two end-points) has been overcome using DEMD, which is developed on the base of (a) compact difference scheme concepts, and (b) minimum temporal variability for the low-frequency component (i.e., the average of the upper and lower envelopes). Determination of either the upper or the lower envelope becomes a well-posed mathematical problem.
(2) DEMD uses hybrid Hermitian polynomials to determine the upper and lower envelopes with the first derivatives at the two end-points (q_L, q_R) as parameters. A set of two algebraic equations for (q_L, q_R) is derived on the base of the minimal integrated absolute value of the third-order derivative (equivalent to minimal temporal variability). The upper and lower envelopes are obtained after the optimal (q_L, q_R) are determined.
(3) The capability of DEMD for eliminating the end effect and detrend uncertainty is demonstrated using a time series consisting of a quadratic trend and four harmonics. A numerical experiment demonstrates that the new approach could indeed eliminate the end effect and detrend uncertainty effectively, with low RRMSEs. The potential advantage of DEMD over postprocessing approaches is that the sum of all IMFs is always the same as the original signal using DEMD, and is usually different from the original signal using postprocessing approaches.
(4) The three synthetic sine waves are used as an example to show the capability of DEMD, since exact components exist for the error estimation. Further justification using real-world examples is needed, although this is difficult because exact components are usually unknown.

Acknowledgments

Peter C. Chu and Chenwu Fan have been supported by the Office of Naval Research (N0001413WX20928) and the Naval Oceanographic Office (N6230612PO00123). N.E. Huang has been supported by a grant NSC 100-2119-I-008-100 (I-RiCE) from the National Science Council, Taiwan.

References

[1] N.E. Huang, Z. Shen, S.R. Long, M.C. Wu, H.H. Shih, Q. Zheng, N.-C. Yen, C.C. Tung, H.H. Liu, The empirical mode decomposition and the Hilbert spectrum for nonlinear and nonstationary time series analysis, Proc. R. Soc. Lond. Ser. A 454 (1998) 903–993.
[2] Z. Wu, N.E. Huang, Ensemble empirical mode decomposition: a noise-assisted data analysis method, Adv. Adapt. Data Anal. 1 (2009) 1–41.
[3] J. Zhao, D. Huang, Mirror extending and circular spline function for empirical mode decomposition method, J. Zhejiang Univ. Sci. Ed. 2 (2001) 247–252.
[4] J. Wang, Y. Peng, X. Peng, Similarity searching based boundary effect processing method for empirical mode decomposition, IEEE Electr. Lett. 43 (1) (2007) 58–59.
[5] R. Faltermeier, A. Zeiler, I.R. Keck, A.M. Tome, A. Brawanski, E.W. Lang, Sliding empirical mode decomposition, in: Proceedings of the IEEE 2010 International Joint Conference on Neutral Network, IJCNN, 2010, pp. 1–8.
[6] B. Weng, K.E. Barner, Optimal and bidirectional optimal empirical mode decomposition, in: Proceedings of the IEEE International Conference on Acoustics, Speech, and Signal Processing, ICASSP'07, vol. III, 2007, pp. 1501–1504.
[7] P.C. Chu, C.W. Fan, N. Huang, Compact empirical mode decomposition—an algorithm to reduce mode mixing, end effect, and detrend uncertainty, Adv. Adapt. Data Anal. 4 (2012). http://dx.doi.org/10.1142/S1793536912500173.
[8] P.C. Chu, C.W. Fan, A three-point combined compact difference scheme, J. Comput. Phys. 140 (1998) 370–399.
[9] P.C. Chu, C.W. Fan, A three-point non-uniform combined compact difference scheme, J. Comput. Phys. 148 (1999) 663–674.
[10] N.E. Huang, Z. Wu, S.R. Long, K.C. Arnold, K. Blank, T.W. Liu, On instantaneous frequency, Adv. Adapt. Data Anal. 1 (2009) 177–229.
[11] N.E. Huang, X. Chen, M.T. Lo, Z. Wu, On Hilbert spectral representation: a true time-frequency representation for nonlinear and nonstationary data, Adv. Adapt. Data Anal. 3 (2011) 63–93.